Reconsidering Six-Degree-of-Freedom Magnetic Actuation Across Scales

Colton R. Thornley, Lan N. Pham, and Jake J. Abbott

***Abstract*—Magnetic actuation, also known as magnetic manipulation, refers to the use of controlled magnetic fields, generated by electromagnets or permanent magnets, to impart forces and torques on a remote magnetic object. The magnetic object is typically modeled as a magnetic dipole, affording five-degree-of-freedom (5-DOF) actuation, comprising 3-DOF force and 2-DOF torque. A method was proposed that uses a three-magnet object in which one magnet is used for traditional 5-DOF actuation and two auxiliary magnets achieve the sixth (torque) DOF via a force couple, and this object can still be modeled and controlled as if it exists at a single point in space, as in traditional 5-DOF actuation. We reconsider this method of 6-DOF magnetic actuation. We perform a numerical study of torque that can be generated on a multi-magnet object of varying shape (but assuming that the individual magnetization vectors are coplanar), size, and orientation, using a variety of well conditioned magnetic manipulation systems. We find that, in the limit as the magnetic object is reduced in size, there is an optimal arrangement of the magnetic object, which is invariant to the manipulation system. We find that the sixth DOF comes at a cost to the original 5-DOF, reducing them by 61% when using the optimal magnetic arrangement; this value is also invariant to the manipulation system. Finally, we find that the sixth DOF scales poorly relative to the other five as the size of the object is reduced, but can be relatively large as we consider objects that are large relative to the distances over which they are being actuated.**

***Index Terms*—Dexterous manipulation, haptics and haptic interfaces, medical robots and systems, micro/nano robots.**

I. Introduction

MAGNETIC ACTUATION, which is also known as magnetic manipulation, refers to the use of controlled magnetic fields, generated by electromagnets or permanent magnets, to impart forces and torques on a remote magnetic object, typically to control its pose (i.e., its position and orientation). Much of the research in magnetic actuation has been motivated by the control of microrobots, which have the potential to be useful for a variety of *in vivo* medical procedures [1] and micromanipulation tasks under the guidance of an optical microscope [2]. There are many other non-microrobotic applications of magnetic actuation, such as magnetic catheters/endoscopes [3]–[5], magnetic capsule endoscopes [6], [7], and untethered magnetic haptic interfaces [8], [9]. In this work, we will simply refer to the magnetic object being acted upon as the magnetic *tool*, without any specific reference to its application.

The simplest model of a magnetic tool is a magnetic dipole, $\mathbf{m}\{\mathrm{A{\cdot}m^2}\}$, which has both a magnitude (proportional to its volume and to the strength of the magnetization of the material, $M\{\mathrm{A{\cdot}m^{-1}}\}$) and a direction (which points from the "south pole" to the "north pole"). All magnetic tools can be approximated by a dipole from sufficient distances relative to their size [10]. Uniformly magnetized spheres can be approximated by a dipole at any distance [10], and a tool that has a geometry and magnetization that can be accurately approximated by a uniformly magnetized sphere can also be accurately approximated by a dipole [11]. In the case of magnetic manipulation of a permanent-magnet tool, the dipole magnitude can be assumed to be constant. When a dipole $\mathbf{m}$ is placed in a magnetic field described by the vector $\mathbf{b}\{\mathrm{T}\}$, the torque $\boldsymbol{\tau}\{\mathrm{N{\cdot}m}\}$ acting on the dipole is calculated as

$$\boldsymbol{\tau} = \mathbf{m} \times \mathbf{b}, \tag{1}$$

and the force $\mathbf{f}\{\mathrm{N}\}$ acting on the dipole is calculated as

$$\mathbf{f} = \begin{bmatrix} \dfrac{\partial \mathbf{b}}{\partial x} & \dfrac{\partial \mathbf{b}}{\partial y} & \dfrac{\partial \mathbf{b}}{\partial z} \end{bmatrix}^T \mathbf{m}. \tag{2}$$

That is, the torque on a dipole is due to the field (as the dipole attempts to rotate to align itself with the field), and the force on a dipole is due to the spatial derivative of the field (as the dipole attempts to translate to achieve a more favorable magnetic energy). The dipole is typically assumed to be at the center-of-mass of the tool, and the magnetic field and its spatial derivatives are calculated at that location as well.

It is typically assumed that only five-degree-of-freedom (5-DOF) magnetic actuation is possible, comprising 3-DOF force (i.e., translation) and 2-DOF torque (i.e., rotation). This falls short of the 6-DOF that would be required for complete control of the pose, but for a tool that is modeled as a dipole it is not possible to generate torque about the dipole-moment axis due to the cross product in (1).

One way to achieve 6-DOF magnetic actuation of a tool is to rigidly embed more than one magnetic object (i.e., dipole) at distinct locations in the tool [12]. Since each magnetic object will be at a distinct location in the applied field, the synthesis of the respective 5-DOF actuations can be used to achieve the desired 6-DOF actuation on the rigid body. In practice,

Manuscript received September 10, 2018; accepted February 15, 2019. Date of publication March 4, 2019; date of current version March 15, 2019. This letter was recommended for publication by Associate Editor S. Regnier and Editor Y. Sun upon evaluation of the reviewers' comments. This work was supported by the National Science Foundation under Grant 1423273. *(Corresponding author: Jake J. Abbott.)*

The authors are with the Department of Mechanical Engineering and the Robotics Center, University of Utah, Salt Lake City, UT 84112 USA (e-mail: colton.thornley@utah.edu; lan.pham@utah.edu; jake.abbott@utah.edu).

Digital Object Identifier 10.1109/LRA.2019.2902742

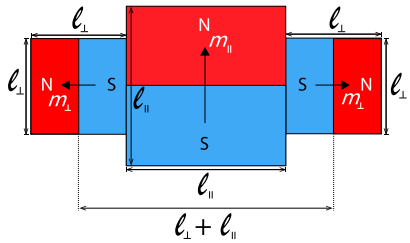

Fig. 1. The three-magnet tool proposed by Diller *et al.* [13]. We model the main central magnet by the dipole $\mathbf{m}_{\parallel}$, and the two auxiliary magnets by the dipole $\mathbf{m}_{\perp}$. We use the lengths $\ell_{\parallel}$ and $\ell_{\perp}$ to describe the size of the respective magnets, which we assume to be either cubes or cylinders (although [13] did not restrict the method to these magnet geometries).

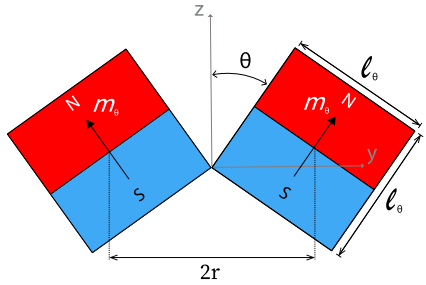

Fig. 2. The magnetic tool considered in this letter, comprising two cubic or cylindrical permanent magnets of dimension ℓ_θ and magnetic dipoles $\mathbf{m}_\theta$ that touch along one edge, with a relative orientation described by the half-angle θ.

this requires that there are enough DOF in control inputs (e.g., electromagnet currents) such that the field and its spatial derivatives can be sufficiently independently prescribed at the respective dipole locations.

Diller *et al.* [13] proposed an innovative and clever alternative method to achieve 6-DOF magnetic actuation for wireless microrobotics that uses the same fundamental physics as the 6-DOF method described above, but maintains the spirit of how magnetic actuation is typically performed: with the tool modeled as existing at a single point in space, and the field and field derivatives calculated at only that single point. In their method, the original permanent-magnet dipole, which we will call $\mathbf{m}_{\parallel}$ (since it tends to align itself parallel with the magnetic field), is augmented by attaching an additional pair of permanent-magnet dipoles, which we will call $\mathbf{m}_{\perp}$, which are antiparallel with each other and are perpendicular to $\mathbf{m}_{\parallel}$, as depicted in Fig. 1. The original 5-DOF actuation is still performed on $\mathbf{m}_{\parallel}$, but it is now possible to use spatial derivatives in the field to apply a force couple to the two $\mathbf{m}_{\perp}$ magnets, resulting in a torque about the axis of $\mathbf{m}_{\parallel}$. The forces generated on the two $\mathbf{m}_{\perp}$ magnets are in opposite directions due to the magnets having opposite polarity in a field with a nominal spatial derivative, not because the spatial derivatives in the field can be independently prescribed at the two locations. In fact, they are both assumed to be at the location of the center-of-mass of $\mathbf{m}_{\parallel}$ for the purpose of field and field-derivative calculation (although their separation distance is critical to generate a torque via the force couple). For this three-magnet tool, the independent torque and force equations (1)–(2) are replaced by a set of coupled 6-DOF torque-force equations, as described in [13].

However, when considering the actuation authority on a magnetic tool, it can be misleading to simply add two new magnets to an existing magnet, since it fundamentally changes the size and mass of the tool. Augmenting a magnetic tool with two new magnets should really be thought of as a reorganization of the existing magnetic material, taking material (and strength) away from $\mathbf{m}_{\parallel}$ in order to form the two new dipoles, which comes at a cost to the original 5-DOF actuation.

In this letter, we reconsider the 6-DOF magnetic actuation method of [13]. First, we describe a two-magnet tool that is equivalent to the three-magnet tool described above, but enables us to vary the design of the tool while controlling for the amount of magnetic material. Next, we describe six different well conditioned magnetic manipulation systems that we will use to evaluate 6-DOF magnetic actuation. Next, we perform an exhaustive numerical study in which we vary the shape, size, and orientation of the two-magnet tool within each of the magnetic manipulation systems; we quantify the ability to generate 3-DOF torque for each combination. We perform an optimization study to maximize the weakest torque DOF, and then we determine how large it is in comparison to the other two. We report on the optimal two-magnet tool design that exists in the limit as the size of the tool is reduced relative to the distance over which it is being manipulated. We quantify how adding the new torque DOF impacts the magnitude of the original 5-DOF force-torque for this optimal design. We also find that the optimal design is invariant to the magnetic manipulation systems considered. Finally, we find that the sixth DOF does not scale favorably as the tool is reduced in size, but can be relatively large as we consider tools that are large relative to the distances over which they are actuated.

II. Methods

A. Magnetic Tool

The magnetic tool that we will consider in this letter comprises two cubic or cylindrical permanent magnets that touch along one edge (Fig. 2). Each magnet of the tool is modeled as a magnetic dipole $\mathbf{m}_\theta$ that resides in the center of the respective magnet. The half-angle θ describes the relative orientations of the two dipoles. By modeling the tool in this way, rather than using a three-magnet tool of Fig. 1, by varying only θ we are effectively able to vary the strengths $\|\mathbf{m}_{\parallel}\|$ and $\|\mathbf{m}_{\perp}\|$ while controlling for the total amount of magnetic material in the tool. For this study, we will consider arrangements between $\theta = 0^\circ$ (i.e., parallel, which is equivalent to having no $\|\mathbf{m}_{\perp}\|$) and $\theta = 90^\circ$ (i.e., antiparallel, which is equivalent to having no $\|\mathbf{m}_{\parallel}\|$). In Appendix A, we discuss the equivalence of three-magnet and two-magnet tools.

B. Magnetic Manipulation Systems

In order to ensure that the conclusions that we draw from this study are not anecdotal or somehow manipulation-system specific, we will consider six distinct configurations of electromagnets for our magnetic manipulation system. Since it is known that at least eight electromagnets are required to ensure

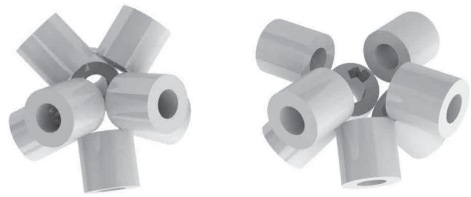

(a) Square-antiprism (b) OctoMag

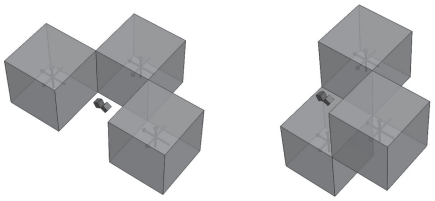

(c) Omnimagnet 3a (d) Omnimagnet 3b

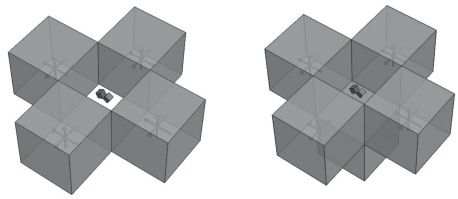

(e) Omnimagnet 4 (f) Omnimagnet 5

Fig. 3. The magnetic manipulation system configurations considered in our numerical simulations.

complete control authority over the magnetic field and its spatial derivatives at a given point in the manipulation workspace [14], all of the configurations that we consider comprise at least eight electromagnets.

The first two configurations that we consider comprise exactly eight electromagnets. The first configuration is the "square antiprism" [15], which is the (approximate) configuration used in the work of Diller *et al.* [13], comprising four electromagnets below a common plane and four electromagnets above a common plane, with each electromagnet at an angle of 30° from the common plane, with the lower set rotated by 45° with respect to the upper set, and with all of the electromagnets having axes pointing toward the common center of the workspace (Fig. 3a). The second configuration is the "OctoMag" configuration [16], which is another well conditioned magnetic manipulation system, comprising four electromagnets in a common plane, four electromagnets below that common plane at an angle of 45° from the plane, with the lower set rotated by 45° with respect to the upper set, and with all of the electromagnets having axes pointing toward the common center of the workspace (Fig. 3b). Note that we use terms such as "below" in reference to the figures, but there is no real sense of vertical in either design.

In addition to the two eight-electromagnet configurations, we also consider four configurations using Omnimagnets (Figs. 3c–3f). An Omnimagnet comprises three mutually orthogonal and independent electromagnets that fit within a cubic package [17]. The Omnimagnet configurations enable us to consider systems with more than eight electromagnets. In all of the configurations, the Omnimagnets are all the same size, and they are configured so that they touch on their edges, which has the effect of making a manipulation workspace that is comparable in size to the Omnimagnets themselves.

In all six configurations, we use simple dipole approximations to model the fields of the electromagnets, with each dipole located at the center-of-mass of the respective electromagnet, which is sufficient to answer our questions of interest. In recent work [15], it was found that workspace conditioning of magnetic manipulation systems is quite insensitive to the specific geometry (and resulting field) of the electromagnets.

C. Torque on a Two-Magnet Tool

For a given magnetic tool, the torque is a function of the magnetic field where the tool resides. The magnetic field $\mathbf{b}$ generated by a dipole source $\mathbf{m}_s$ is

$$\mathbf{b}(\mathbf{p}) = \frac{\mu_0}{4\pi\|\mathbf{p}\|^5}(\mathbf{p}\mathbf{p}^T - I\|\mathbf{p}\|^2)\mathbf{m}_s, \tag{3}$$

where $\mathbf{p}\{\mathrm{m}\}$ is the vector describing the location of $\mathbf{b}$ with respect to $\mathbf{m}_s$, $\mu_0 = 4\pi \times 10^{-7}$ N·A^{-2} is the permeability of free space, and I is a 3×3 identity matrix.

The total torque calculation for a tool that comprises two magnets is then

$$\boldsymbol{\tau} = \sum_{i=1}^{2}\left((\mathbf{m}_i \times \mathbf{b}_i) + (\mathbf{r}_i \times \mathbf{f}_i)\right), \tag{4}$$

where $\mathbf{m}_i$ is the dipole moment of the ith magnet of the tool, $\mathbf{b}_i$ is the applied field at the center-of-mass of the ith magnet, $\mathbf{r}_i\{\mathrm{m}\}$ is the vector from the center-of-mass of the tool to the center-of-mass of the ith magnet, and $\mathbf{f}_i$ is the force acting on the ith magnet calculated using (2). In this letter, the actual spatial derivatives of the field in (2) are calculated using the central-difference method, utilizing (3). The contribution of the $\mathbf{r}_i \times \mathbf{f}_i$ term is what provides the force couple that enables 6-DOF actuation. Note: we are still modeling each of the individual magnets as dipoles, which is an approximation in general; this model is experimentally validated in Appendix B.

D. Quantifying Torque Generation

For a given magnetic tool in a given pose in the manipulation workspace, one can construct an actuation matrix that maps the array of n electric currents through the electromagnets to the torque acting on the tool [16]. An alternative but less common formulation, which we will use here, uses an actuation matrix $T\{\mathrm{N{\cdot}A^{-1}{\cdot}m^{-1}}\}$ that maps the array of n dipole magnitudes of the electromagnets $\mathscr{M} = [m_1 \ldots m_n]^T$ to the torque acting on the tool:

$$\boldsymbol{\tau} = T\mathscr{M}. \tag{5}$$

This formulation results in a T matrix that generalizes better, without being sensitive to the particular design of the electromagnets. We can use the singular value decomposition (SVD) to decompose T as

$$T = U\Sigma V^T, \tag{6}$$

where the input singular vectors are the columns of the orthonormal $V = [\mathbf{v}_1 \ \ldots \ \mathbf{v}_n]$, the output singular vectors are the

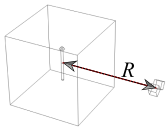

Fig. 4. The distance R from the dipole of the electromagnet to the centroid of the tool, shown (for example) with respect to an Omnimagnet.

columns of the orthonormal $U = [\mathbf{u}_1 \quad \mathbf{u}_2 \quad \mathbf{u}_3]$, and the singular value matrix Σ is of the form

$$\Sigma = \begin{bmatrix} \sigma_1 & 0 & 0 & 0 & & 0 \\ 0 & \sigma_2 & 0 & 0 & \cdots & 0 \\ 0 & 0 & \sigma_3 & 0 & & 0 \end{bmatrix}. \tag{7}$$

The singular values, σ_1 through σ_3, describe the relative strength of the torque in the three orthogonal directions of the output singular vectors, which do not necessarily correspond to the principal axes of the tool or the workspace.

In the case of traditional 5-DOF magnetic actuation (i.e., 2-DOF torque and 3-DOF force) of a single magnetic dipole, $\sigma_3 = 0$ and $\mathbf{u}_3$ corresponds to the magnetization direction, and $\sigma_2 \leq \sigma_1$. In the case of 6-DOF magnetic actuation, $\sigma_3 \neq 0$ in general. We can use a performance index to evaluate the relative strength of the torque that can be generated in the three orthogonal directions of the tool:

$$\kappa = \frac{\sigma_3}{\sigma_2} \tag{8}$$

κ compares the weakest torque direction to the second-strongest (also second-weakest) torque direction. $\kappa = 1$ indicates a high degree of isotropy in torque generation (acknowledging that even in the case of traditional 5-DOF magnetic actuation, torque generation is not perfectly isotropic since $\sigma_2 \leq \sigma_1$). $\kappa = 0$ if there is no torque generation possible in (at least) one direction, but that direction need not exclusively correspond to the z axis of the tool in Fig. 2.

E. Dimensional Analysis

When we consider κ, the results are dimensionless and thus generalize well, but that is not the case with σ_3. We can make use of the Buckingham Π theorem [18] to obtain nondimensional terms that will help us interpret and generalize our results with respect to the output variable $\sigma_3\{\mathrm{N{\cdot}A^{-1}{\cdot}m^{-1}}\}$. We know that σ_3, for any given system and tool pose, is a function of four independent input variables: magnetization $M\{\mathrm{A{\cdot}m^{-1}}\}$, size $\ell_\theta\{\mathrm{m}\}$, distance $R\{\mathrm{m}\}$ (see Fig. 4), and permeability $\mu\{\mathrm{N{\cdot}A^{-2}}\}$ (we are only interested in $\mu = \mu_0$). The dimensions in those variables are N, M, and A. With five variables and three dimensions, there are $5 - 3 = 2$ different dimensionless Π groups that fully describe the physics:

$$\Pi_0 = f(\Pi_1) \quad \text{where} \quad \Pi_0 = \frac{\sigma_3}{\mu_0 M} \quad \text{and} \quad \Pi_1 = \frac{R}{\ell_\theta} \tag{9}$$

F. Tool-System Combinations Considered

A wide variety of tool shapes and sizes are considered. We only explicitly consider tools comprising cubic magnets, but the results for $\sigma_3/(\mu_0 M)$ can simply be scaled by a factor of $\pi/4$ to consider cylindrical magnets. We vary the ratio R/ℓ_θ from 2 (a very large tool) to 256 (a very small tool) in powers of 2 (see Fig. 5), giving a total of eight tool sizes. The value of θ, which is the half angle between the magnets of the tool that parameterizes its shape, is varied from 0° to 90° in increments of 0.2° for all tool sizes except for the smallest, which is varied in increments of 0.1°; this smaller increment is used due to the sensitivity of the numerical computation observed for the smallest tool size. This results in 451 tools for 7 of the tool sizes, and 901 tools for the smallest tool size, giving 4058 distinct tools considered.

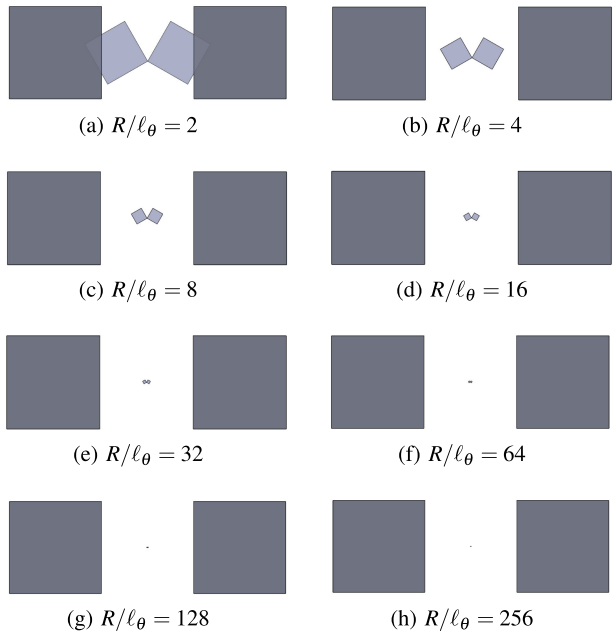

Fig. 5. The eight values for R/ℓ_θ (i.e., normalized distances) considered in the numerical experiment. To help visualize the relative tool size, we depict the specific case of a tool located between two Omnimagnets with a spacing like those in Fig. 3. For $R/\ell_\theta = 2$, the tool appears to collide with the Omnimagnets, but the Omnimagnets are simply modeled as magnetic dipoles at their respective centers.

For each of the tools described above, and each of the magnetic manipulation systems considered, we only consider the tool located in the common center of the workspace, but at that position, a wide variety of tool orientations are considered. To define those orientations, the tool starts with its dipoles both aligned with the system z axis, and then θ causes its dipoles to rotate in the y-z plane (e.g., the dipoles are parallel to the system y axis when $\theta = 90°$). The orientations are then obtained by using all possible combinations of rotating the tool about the x, y, and z system axes, using XYZ Fixed Angles, from 0° to 360° in increments of 45°. This results in 729 poses for each tool-system combination, although some of the poses are duplicates. We subsequently verified that thorough coverage of orientations was obtained, by visualizing the equivalent angle-axis formulation of each orientation.

For each of the tool-system-orientation combinations, the torque vector $\boldsymbol{\tau}$ from (4) is calculated on the tool by applying a unit dipole strength in each of the electromagnets in the system, one at a time, which forms the respective column of

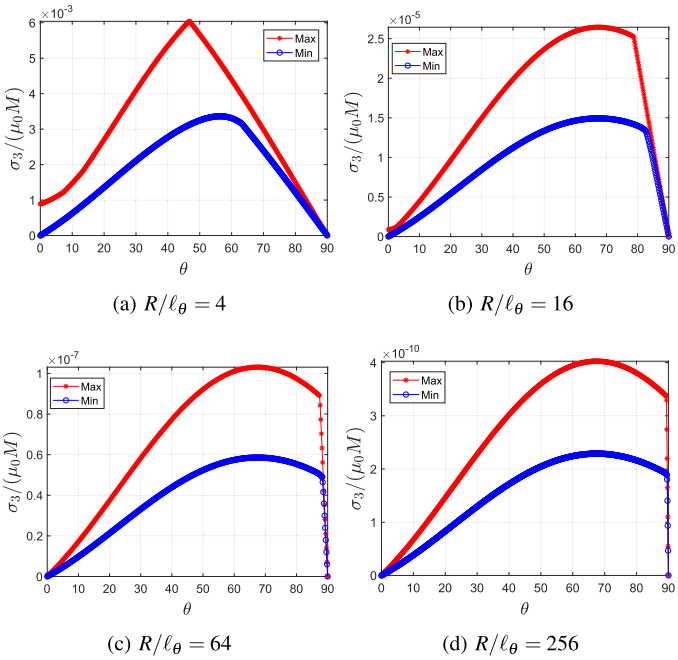

(a) $R/\ell_\theta = 4$ (b) $R/\ell_\theta = 16$

(c) $R/\ell_\theta = 64$ (d) $R/\ell_\theta = 256$

Fig. 6. The maximum and minimum performance index $\sigma_3/(\mu_0 M)$ over all tool poses, as a function of θ, simulated in the Omnimagnet-5 configuration.

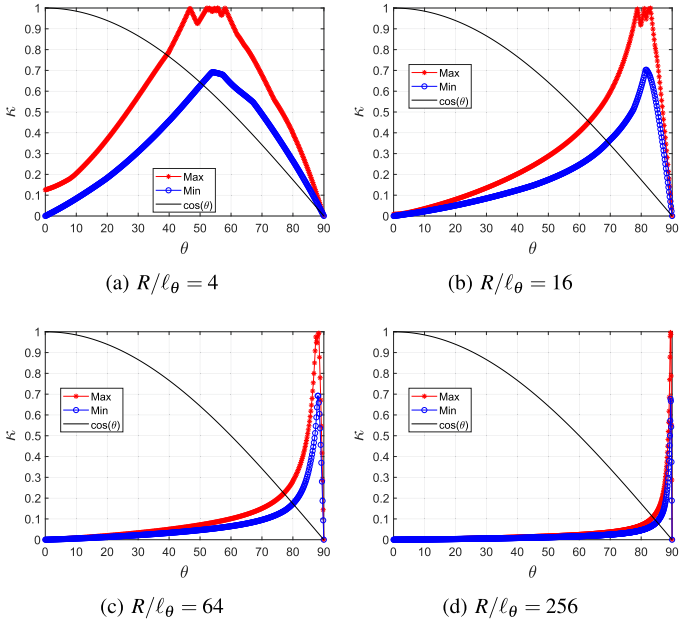

(a) $R/\ell_\theta = 4$ (b) $R/\ell_\theta = 16$

(c) $R/\ell_\theta = 64$ (d) $R/\ell_\theta = 256$

Fig. 7. The maximum and minimum performance index κ over all tool poses, as a function of θ, simulated in the Omnimagnet-5 configuration. The $\cos(\theta)$ curve describes the attenuation of the original 5-DOF force-torque, since only the $\cos(\theta)$ component of each $\mathbf{m}_\theta$ contributes to the original 5-DOF (i.e., to the effective $\mathbf{m}_\parallel$).

the T matrix in (5). In the end, we compute a full T matrix for each tool-system-orientation combination. After completing the torque simulations and forming the T matrices, they are post-processed to calculate the SVD and the performance indices. All simulations are performed in MATLAB.

G. Optimization

Finally, we perform a study in which the weakest direction of the 3-DOF torque vector (i.e., σ_3)) is maximized. For each manipulation-system configuration and dimensionless size, this was performed as a maximin optimization of nondimensionalized σ_3 as follows:

$$\theta^* = \arg\max_{\theta} \min_{\psi} \frac{\sigma_3}{\mu_0 M}(\theta, \psi), \tag{10}$$

where θ is the half-angle of the tool, ψ describes the orientation of the tool, and θ^* is the maximin-optimal θ. That is, for each θ of a given tool-system combination, we find the tool orientation that has the lowest (i.e., poorest) σ_3. Then, we search over all of those worst-case σ_3 values to determine the value for θ for which σ_3 is the largest. We determine this value of θ to be optimal in the sense that it makes the tool have as large a torque-generation capability as possible in the weakest torque direction and worst-case tool orientation, which is a conservative estimate of the torque generation generally.

III. Results

In Figs. 6 and 7 we present the complete results of our simulation study (for brevity) for the Omnimagnet-5 configuration for four nondimensional tool sizes. For both $\sigma_3/(\mu_0 M)$ and κ, we present the worst-case ("Min") and best-case ("Max") values found across all of the tool orientations considered. These curves are typical of all of the magnetic manipulation systems considered, but the Omnimagnet-5 configuration resulted in the highest values of $\sigma_3/(\mu_0 M)$, which is not surprising considering it has the highest number of electromagnets.

We note that optimizing for $\sigma_3/(\mu_0 M)$ and κ are two distinct goals. One way to make κ appear good (i.e., close to 1) is to have σ_3 and σ_2 be equally poor, which is not a desirable outcome. This motivates our belief that $\sigma_3/(\mu_0 M)$ is the most important performance index that we consider.

We see that if the tool is large with respect to the magnetic manipulation system, it is possible to achieve a relatively good κ without drastically sacrificing force-torque generation in the original 5-DOF. For example, with $R/\ell_\theta = 16$ and $\theta = 60^\circ$ it is possible to achieve a torque in the weakest DOF that is close to the maximum possible across θ and is 25–40% (depending on tool orientation) as strong as the second-strongest torque direction, while only attenuating the original 5-DOF force-torque by 50%. However, as R/ℓ_θ becomes larger, the conditioning becomes increasingly poor unless we are willing to drastically attenuate the original 5-DOF.

Figure 8 presents the complete results of the optimization study described in Section II-G. Note that these values correspond to the peak values of the "Min" curves in the respective data sets represented by Fig. 6. A few things are immediately evident from the plots in Fig. 8. We see that there is an asymptotic nature to the results as R/ℓ_θ increases, which can be interpreted as the size of the tool shrinking within a given magnetic manipulation system. The optimal θ approaches 67° as the tool gets smaller (Fig. 8b). There is a corresponding reduction of the effective $\|\mathbf{m}_\parallel\|$ value, and thus the original 5-DOF force-torque, by 61% (Fig. 8c).

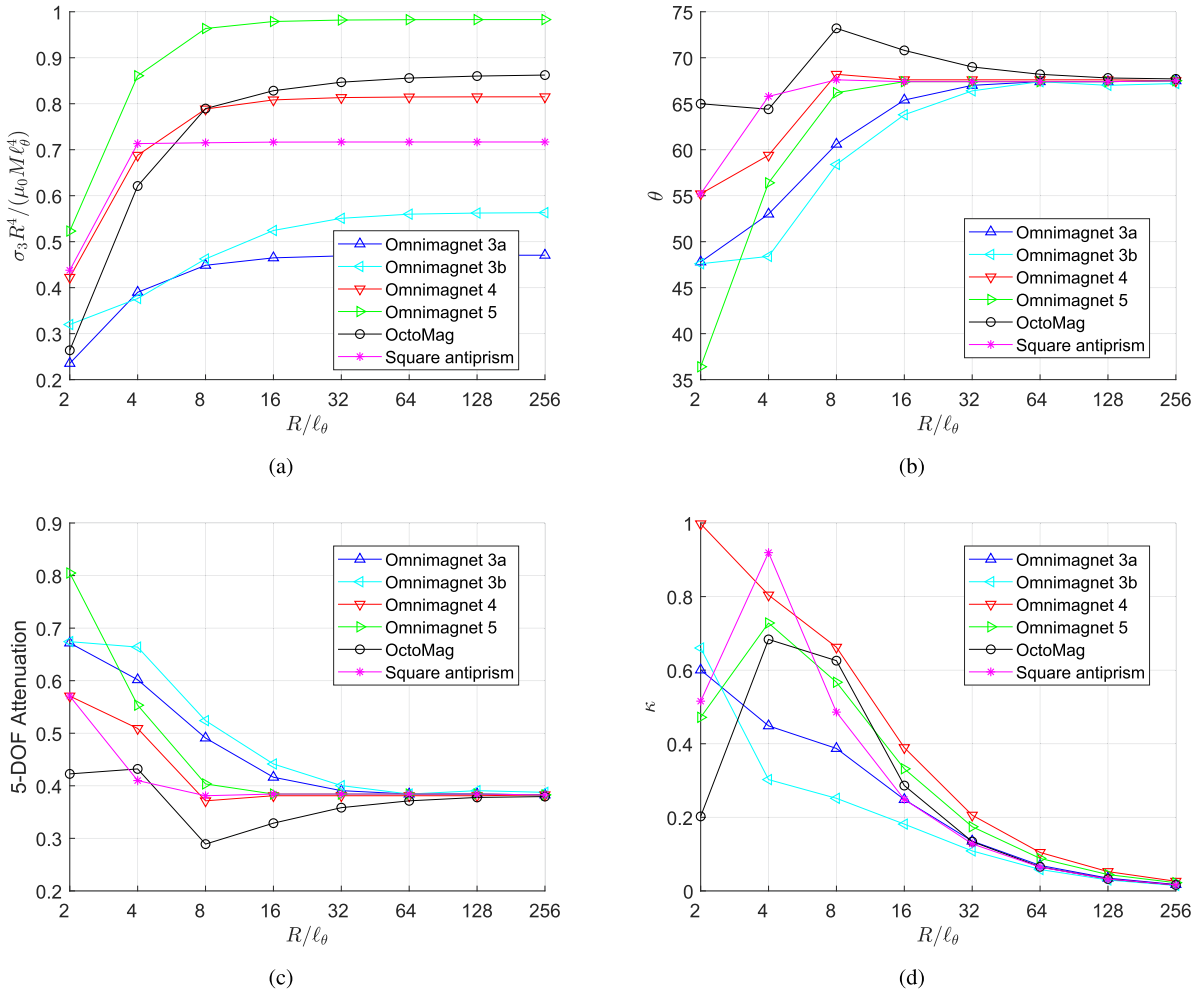

Fig. 8. Optimal $\sigma_3/(\mu_0 M)$ and θ, the resulting attenuation of the original 5-DOF, and the resulting κ, as a function of R/ℓ_θ. Presenting the optimal $\sigma_3/(\mu_0 M)$ normalized by $(R/\ell_\theta)^{-4}$ in (a) clarifies the scaling of $\sigma_3/(\mu_0 M)$ with R/ℓ_θ.

In Fig. 8a, we choose to plot the optimal $\sigma_3/(\mu_0 M)$ normalized by $(R/\ell_\theta)^{-4}$ (which results in asymptotes to distinct constant values as R/ℓ_θ increases) because we observed that the optimal $\sigma_3/(\mu_0 M)$ decayed asymptotically to zero as $\sim (R/\ell_\theta)^{-4}$. In general, we expect torque to become weaker as the tool becomes smaller due to a reduction in magnetic material. However, Fig. 8a indicates that the torque generation ability in the weakest direction scales as $\sim \ell_\theta^4$, rather than the $\sim \ell_\theta^3$ that would be expected from volumetric scaling. Ultimately, this is due to the fact that the separation distance between the magnets, which is required to generate the sixth-DOF force couple, is also getting smaller.

In addition, as the tool becomes smaller, σ_3 gets smaller faster than σ_2 (Fig. 8d), so isotropy in torque generation diminishes asymptotically to zero. For example, for $R/\ell_\theta = 256$, κ is less than 0.05, meaning that the torque-generation capability in direction $\mathbf{u}_3$ is less than 5% of the torque-generation capability in the direction $\mathbf{u}_2$.

For devices that are small in comparison to their distance from the magnetic-field sources, there is very little difference between manipulation systems when considering the trends of Fig. 8, except to say that some systems are somewhat better suited to 6-DOF actuation than others (Fig. 8a). As a result, we believe that we can draw conclusions regarding 6-DOF magnetic actuation of relatively small tools without consideration of the particular magnetic manipulation system being used. Our results indicate that 6-DOF magnetic actuation does not scale favorably for small tools (e.g., microrobots). The extra torque DOF will be weak relative to the other 2-DOF torque, and adding the extra DOF of torque comes at a substantial cost to the original 5-DOF control authority.

IV. Conclusion

In this letter, we reconsidered a previously proposed method of 6-DOF magnetic actuation for wireless magnetic tools [13]. We used a two-magnet tool that enabled us to control for the amount of magnetic material in the tool while allocating it between the component responsible for the traditional 5-DOF force-torque actuation and the new sixth (torque) DOF. We showed that this tool is equivalent to the three-magnet tool proposed in [13]. We considered six different magnetic

manipulation systems with well conditioned workspaces. We created a numerical model with which the torques generated on the tool for varying shape, size, and orientation are obtained for all of the magnetic manipulation systems. We quantified the generation of torque and identified how isotropic these torques are and determined the cost that is incurred on the original 5-DOF actuation in order to obtain the new sixth DOF. We also experimentally verified that the model used to calculate torque on the two-magnet tool.

We found that, in the limit as the magnetic tool is reduced in size, there is an optimal magnetic arrangement of the tool (a half-angle of $\theta = 67^\circ$), which is invariant to the manipulation system used (assuming a sufficiently well conditioned system). We found that the sixth DOF comes at a cost to the original 5-DOF, reducing them by 61% when using the optimal tool; this value is also invariant to the manipulation system. Finally, we find that the sixth DOF scales poorly as the size of the tool is reduced, but can be relatively large as we consider tools that are large relative to the distances over which they are being manipulated. It should be noted that our study only considered tools comprising magnets with individual magnetizations that are coplanar (as in [13]), and does not consider more complicated arrangements (e.g., three mutually orthogonal magnets).

Appendix A
Equivalence Between Two-Magnet and Three-magnet Tools

There is an approximate equivalence between a given two-magnet tool of the design of Fig. 2 with $\|\mathbf{m}_\theta\|$, ℓ_θ, M, and θ known, and some three-magnet tool of the design of Fig. 1. First, we can calculate the equivalent $\|\mathbf{m}_\parallel\|$:

$$\|\mathbf{m}_\parallel\| = 2\cos(\theta)\|\mathbf{m}_\theta\| \tag{11}$$

The equivalent $\|\mathbf{m}_\perp\|$ is constrained by the equivalence of the force couple used to generate the new torque DOF as

$$(\ell_\parallel + \ell_\perp)\|\mathbf{m}_\perp\| = 2r\|\mathbf{m}_\theta\|\sin(\theta), \tag{12}$$

where $\ell_\parallel + \ell_\perp\{\mathrm{m}\}$ is the distance between the two $\mathbf{m}_\perp$ dipoles in the three-magnet tool (see Fig. 1), and $2r\{\mathrm{m}\}$ is the distance between the two $\mathbf{m}_\theta$ dipoles in the two-magnet tool (see Fig. 2). The distance r is

$$r = \frac{\ell_\theta}{\sqrt{2}}\sin\left(\theta + \frac{\pi}{4}\right). \tag{13}$$

Assuming the same magnetization M of the magnetic material for both tools provides the constraint

$$M = \frac{\|\mathbf{m}_\parallel\|}{c_\parallel \ell_\parallel^3} = \frac{\|\mathbf{m}_\perp\|}{c_\perp \ell_\perp^3} = \frac{\|\mathbf{m}_\theta\|}{c_\theta \ell_\theta^3} \tag{14}$$

where $c_i = 1$ for a cubic magnet, and $c_i = \pi/4$ for a cylindrical magnet. We can use (14) to find $\ell_\parallel$:

$$\ell_\parallel = \left(\frac{\|\mathbf{m}_\parallel\|}{c_\parallel M}\right)^{1/3} \tag{15}$$

and to find $\|\mathbf{m}_\perp\|$:

$$\|\mathbf{m}_\perp\| = M c_\perp \ell_\perp^3 \tag{16}$$

TABLE I
Parameters of the Six Two-Magnet Tools

Parameter	Tool 1	Tool 2	Tool 3	Tool 4	Tool 5	Tool 6
$\ell_\theta\{\mathrm{mm}\}$	12.7	12.7	12.7	9.53	9.53	9.53
θ	27°	47°	67°	27°	47°	67°
$\|\mathbf{m}_\theta\|\{\mathrm{A}\cdot\mathrm{m}^2\}$	2.4	2.4	2.4	0.97	0.97	0.97

where $\ell_\perp$ is still unknown. Substituting (16) into (12) and rearranging results in

$$M c_\perp \ell_\perp^4 + M c_\perp \ell_\parallel \ell_\perp^3 - 2r\|\mathbf{m}_\theta\|\sin(\theta) = 0 \tag{17}$$

where $\ell_\perp$ is the only unknown. This is a fourth-order polynomial of $\ell_\perp$, and its positive real root is the solution for $\ell_\perp$. Finally, this value is used in (16) to complete the equivalent three-magnet tool of Fig. 1.

Appendix B
Experimental Verification of Two-Magnet-Tool Torque Model

All of the numerical studies performed in this letter assume accuracy of the magnetic models used. The equations that govern magnetic manipulation are well understood and have been shown many times to provide accurate descriptions for what is observed experimentally, but they are typically only used to describe the manipulation of a single magnetic dipole (e.g., permanent magnet). As a result, it is important to verify that the torques generated on a tool comprising two permanent magnets in close proximity (i.e., the two-magnet tool of Fig. 2) are accurately predicted by the simplified equation (4), which assumes that the magnets are point dipoles (although they really have shape effects), and which assumes that the magnets have no interaction with each other (although "permanent" magnets will effect each other's magnetization to some extent). We expect the small change in magnetization to be a function of θ in general, but not a function of the size of tool (due to the homothetic property of magnetic fields).

We constructed six two-magnet tools, as described in Table I, comprising two different magnet sizes and three different half-angles. The magnets used are made of NdFeB. Their magnetic-dipole values were obtained experimentally by attaching each of the single magnets to an ATI Nano17 6-DOF force-torque sensor, and then applying a magnetic field perpendicular to the dipole of the magnet (using an Omnimagnet of the type described in [19]), and then recording the torque generated. Since the field is perpendicular to the dipole of the magnet, (1) gives $\|\boldsymbol{\tau}\| = \|\mathbf{m}\|\|\mathbf{b}\|$. The field $\mathbf{b}$ was obtained using (3) with the dipole source known. The dipole magnitude is then $\|\mathbf{m}\| = \|\boldsymbol{\tau}\|/\|\mathbf{b}\|$ and magnetization is $M = \|\mathbf{m}\|/\ell^3$, where ℓ is the cubic length of the magnet in question.

We tested each of the six tools in the configuration shown in Fig. 9. We tested each tool at each of the separation distances $R = \{140, 150, 160, 170, 180\}$ mm. For this range, the error in the dipole field model of the Omnimagnet's field is less than 5% [17]. The tools were each held in place using 3D-printed PLA

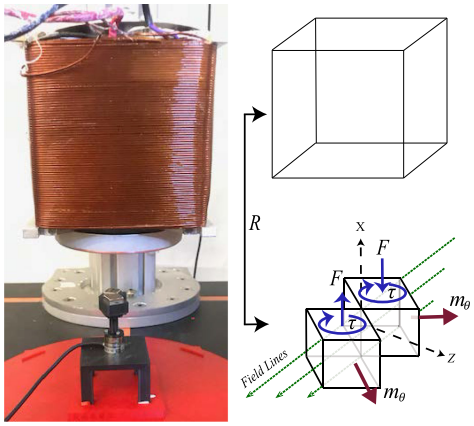

Fig. 9. (a) Experimental setup. (b) Depiction of magnetic forces and torques for traditional and sixth-DOF torque.

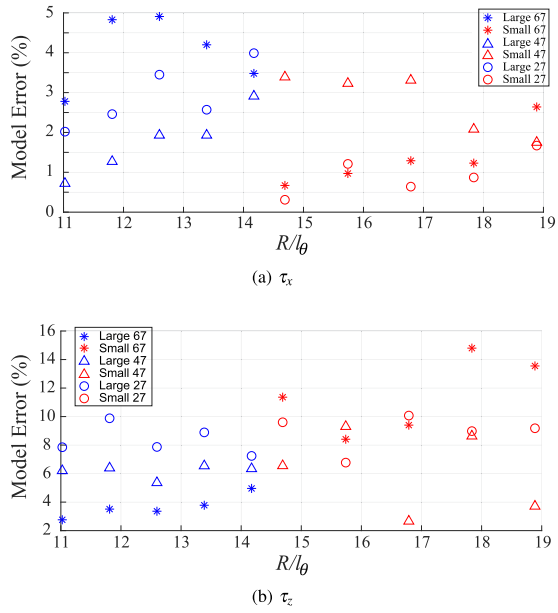

(a) τ_x

(b) τ_z

Fig. 10. Error between model and experimental results for (a) traditional torque about the tool's x axis and (b) sixth-DOF torque about the tool's z axis. See Fig. 9 for definitions.

fixtures, which were then fastened to the ATI Nano17 6-DOF force-torque sensor as shown. We used the Omnimagnet to apply a field of 1.4 mT in the tool's y axis, located at the center-of-mass of the tool, which generates a traditional torque τ_x about the tool's x axis (the sensor measures the sum of the respective torques developed on the two magnets), while it simultaneously generates the sixth-DOF torque τ_z about the tool's z axis as a force couple due to the nonuniformity in the field. There is also a small force developed in the tool's $-y$ axis due to nonuniformity in the field; this force is corrected for when calculating τ_z from the sensor data. We perform each experiment four times and average the results. For each value, we calculate the error in the model of (4) relative to the experimentally measured value.

The results of the validation experiments are shown in Fig. 10. We observed errors throughout the range of 0–15%, with no clear trends in either half-angle θ or actuation distance relative to tool size. Some of the error is attributed to sensitivity to the accuracy of positioning the Omnimagnet. As a result, we may expect to see comparable levels of error in the simulated results of this study, but we do not expect the trends and overall conclusions of this study to be affected.

ACKNOWLEDGMENT

The authors would like to thank A. Pourkand for his assistance in the creation of Fig. 3, and Dr. T. Hermans, Dr. S. Roundy, and the reviewers for their feedback.

REFERENCES

[1] B. J. Nelson, I. K. Kaliakatsos, and J. J. Abbott, "Microrobots for minimally invasive medicine," *Annu. Rev. Biomed. Eng.*, vol. 12, pp. 55–85, 2010.
[2] E. Diller and M. Sitti, "Micro-scale mobile robotics," *Found. Trends Robot.*, vol. 2, no. 3, pp. 143–259, 2013.
[3] J. Edelmann, A. J. Petruska, and B. J. Nelson, "Magnetic control of continuum devices," *Int. J. Robot. Res.*, vol. 36, no. 1, pp. 65–85, 2017.
[4] L. B. Kratchman, T. L. Bruns, J. J. Abbott, and R. J. Webster III, "Guiding elastic rods with a robot-manipulated magnet for medical applications," *IEEE Trans. Robot.*, vol. 33, no. 1, pp. 227–233, Feb. 2017.
[5] P. R. Slawinski, A. Z. Taddese, K. B. Musto, K. L. Obstein, and P. Valdastri, "Autonomous retroflexion of a magnetic flexible endoscope," *IEEE Robot. Autom. Lett.*, vol. 2, no. 3, pp. 1352–1359, Jul. 2017.
[6] H. Keller *et al.*, "Method for navigation and control of a magnetically guided capsule endoscope in the human stomach," in *Proc. IEEE RAS/EMBS Int. Conf. Biomed. Robot. Biomechatronics*, 2012, pp. 859–865.
[7] A. W. Mahoney and J. J. Abbott, "Five-degree-of-freedom manipulation of an untethered magnetic device in fluid using a single permanent magnet with application in stomach capsule endoscopy," *Int. J. Robot. Res.*, vol. 35, no. 1–3, pp. 129–147, 2016.
[8] J. B. Brink, A. J. Petruska, D. E. Johnson, and J. J. Abbott, "Factors affecting the design of untethered magnetic haptic interfaces," in *Proc. IEEE Haptics Symp.*, 2014, pp. 107–114.
[9] S. A. Pedram, R. L. Klatzky, and P. Berkelman, "Torque contribution to haptic rendering of virtual fixtures," *IEEE Trans. Haptics*, vol. 10, no. 4, pp. 567–579, Oct.–Dec. 2017.
[10] E. P. Furlani, *Permanent Magnet and Electromechanical Devices*. San Diego, CA, USA: Academic, 2001.
[11] A. J. Petruska and J. J. Abbott, "Optimal permanent-magnet geometries for dipole field approximation," *IEEE Trans. Magn.*, vol. 49, no. 2, pp. 811–819, Feb. 2013.
[12] P. Berkelman and M. Dzadovsky, "Magnetic levitation over large translation and rotation ranges in all directions," *IEEE/ASME Trans. Mechatronics*, vol. 18, no. 1, pp. 44–52, Feb. 2013.
[13] E. Diller, J. Giltinan, G. Z. Lum, Z. Ye, and M. Sitti, "Six-degree-of-freedom magnetic actuation for wireless microrobotics," *Int. J. Robot. Res.*, vol. 35, no. 1–3, pp. 114–128, 2016.
[14] A. J. Petruska and B. J. Nelson, "Minimum bounds on the number of electromagnets required for remote magnetic manipulation," *IEEE Trans. Robot.*, vol. 31, no. 3, pp. 714–722, Jun. 2015.
[15] A. Pourkand and J. J. Abbott, "A critical analysis of eight-electromagnet manipulation systems: The role of electromagnet configuration on strength, isotropy, and access," *IEEE Robot. Autom. Lett.*, vol. 3, no. 4, pp. 2957–2962, Oct. 2018.
[16] M. P. Kummer, J. J. Abbott, B. E. Kratochvil, R. Borer, A. Sengul, and B. J. Nelson, "OctoMag: An electromagnetic system for 5-DOF wireless micromanipulation," *IEEE Trans. Robot.*, vol. 26, no. 6, pp. 1006–1017, Dec. 2010.
[17] A. J. Petruska and J. J. Abbott, "Omnimagnet: An omnidirectional electromagnet for controlled dipole-field generation," *IEEE Trans. Magn.*, vol. 50, no. 7, p. 8400810, Jul. 2014.
[18] E. Buckingham, "On physically similar systems; illustrations of the use of dimensional equations," *Phys. Rev.*, vol. 4, no. 4, pp. 345–376, 1914.
[19] A. J. Petruska, J. B. Brink, and J. J. Abbott, "First demonstration of a modular and reconfigurable magnetic-manipulation system," in *Proc. IEEE Int. Conf. Robot. Autom.*, 2015, pp. 149–155.